의학석사 학위논문

Multivalent Electrostatic *Pi*-Cation Interactions: The Driving Force of Phase Separation between Synaptophysin and Synapsin

다가 정전기 *Pi*-Cation 상호 작용: Synaptophysin과 Synapsin 사이의 Phase Separation의 원동력

2023 년 8 월

서울대학교 대학원

의과학과 신경과학/생리학 전공

김 고 은

A thesis of the Degree of Master of Philosophy

다가 정전기 *Pi*-Cation 상호 작용: Synaptophysin과 Synapsin 사이의 Phase Separation의 원동력

Multivalent Electrostatic *Pi*-Cation Interactions: The Driving Force of Phase Separation between Synaptophysin and Synapsin

August 2023

The Department of Biomedical Sciences

Seoul National University College of Medicine

Goeun Kim

다가 정전기 *Pi*-Cation 상호 작용: Synaptophysin과 Synapsin 사이의 Phase Separation의 원동력

지도 교수 장 성 호

이 논문을 의학석사 학위논문으로 제출함
2023 년 4 월

서울대학교 대학원
의과학과 신경과학/생리학 전공
김 고 은

김고은의 의학석사 학위논문을 인준함
2023 년 7 월

위 원 장

부위원장

위 원

Abstract

Our group has recently demonstrated that the proteins synaptophysin (Syph) and synapsin (Syn) can undergo a process called liquid–liquid phase separation (LLPS), resulting in the clustering of small synaptic–like microvesicles within living non–neuronal cells, resembling synaptic vesicle (SV) clusters. Despite the absence of direct physical interactions between Syph and Syn, the mechanism underlying their coacervation, or the formation of droplet–like clusters, has remained elusive.

Here, I propose that multivalent electrostatic *pi*–cation interactions play a primary role in their coacervation. The C–terminal region (Ct) of Syph contains ten repeated sequences, with nine starting with tyrosine (Y–G–P/Q–Q–G), known to facilitate phase separation via *pi*–*pi* and *pi*–cation interactions. Additionally, disorder–promoting amino acids, such as glycine, proline, and glutamine, were abundant in the Syph Ct, suggesting a propensity for phase separation.

My findings demonstrate that Syph Ct can undergo LLPS through *pi*–*pi* interactions, but only at non–physiological concentrations *in vitro*. Additionally, it can also undergo phase separation with the help of or additional interactions by combining with light–sensitive CRY2PHR or tagging subunits of a multimeric protein within living cells.

Importantly, mutating the tyrosine residues to serine (referred to as 9YS) abolishes the phase–separating property of Syph Ct,

underscoring the critical role of tyrosine-mediated *pi*-interactions in this process. Moreover, my investigations have revealed that the 9YS mutation prevents the coacervation between Syph and Syn. Notably, since Syph 9YS retains same negative charge of Syph in the cytoplasm, my results strongly suggest that *pi*-cation interactions, rather than simple charge interactions, are responsible for the coacervation of these proteins.

By unraveling the underlying mechanism governing the coacervation of Syph and Syn, my study not only provides valuable insights into the molecular processes at play but also raises the intriguing possibility that the regulation of *pi*-cation interactions between Syph and Syn during synaptic activity may contribute to the dynamic nature of synaptic vesicle clustering.

* This work is published in *Molecular Brain*.

Keyword : Synaptophysin, Synapsin, Liquid-liquid phase separation (LLPS), *pi*-cation interactions, Synaptic vesicle cluster, Presynaptic nerve terminals

Student Number : 2018-12556

Table of Contents

Multivalent Electrostatic *Pi*–Cation Interactions: The Driving Force of Phase Separation between Synaptophysin and Synapsin

List of Figures

List of Abbreviations

1,6-HD: 1,6-Hexanediol

6xHis: Hexahistidine

BSA: Bovine serum albumin

CaMKII α : Ca^{2+}/Calmodulin-dependent kinase II

Ct: C-terminal

CTD: C-terminal domain

DMEM: Dulbecco modified eagle medium

DTT: Dithiothreitol

FBS: Fetal bovine serum

FRAP: Fluorescence recovery after photobleaching

FUS-RBD: FUS RNA binding domain

FUS: Fused in sarcoma

HA: Haemagglutinin

hnRNPA1: Heterogeneous nuclear ribonucleoprotein A1

ICC: Immunocytochemistry

IDR: Intrinsically disordered region

IPTG: Isopropyl- β -D-thiogalactopyranoside

KO: Knockout

LLPS: Liquid-liquid phase separation

mCer: mCerulean

mCh: mCherry

MP: Multimeric protein

NHE6: $Na^+(K^+)/H^+$ exchanger 6

PBS: Phosphate buffered saline

PEG8000: Polyethylene glycol 8000

PFA: Paraformaldehyde

PLD: Prion-like domain

PTM: Post-translational modifications

RT: Room temperature

SVs: Synaptic vesicles

Syn: Synapsin

Syph: Synaptophysin

Tau: Tubulin associated unit

TDP-43: TAR DNA-binding protein 43

VAMP2: Vesicle-associated membrane protein 2

Introduction

Synaptic vesicles (SVs) form tightly packed clusters that are well distinguished from the surrounding cytoplasm. Recent studies have suggested that principles of liquid–liquid phase separation (LLPS) may underlie the organization of such clusters (1, 2). LLPS is a process through which proteins, RNAs, and organelles can self–assemble into biomolecular condensates via multivalent, low–affinity interactions often involving intrinsically disordered regions (IDRs) of the participating proteins (3–5).

Synapsin (Syn), a major constituent of the matrix that connects SVs, was shown to have LLPS properties and to capture small lipid vesicles into its liquid phase *in vitro* (2). I, however, recently found that unlike *in vitro*, Syn alone had a diffuse cytosolic distribution in living cells. I found that co–expression of Syn together with synaptophysin (Syph), an integral tetraspanin SV membrane protein, is required to induce the formation of biomolecular condensates in living cells. These condensates are indeed clusters of small synaptic–like microvesicles, which are highly reminiscent of SV clusters (1). Since there is no direct interaction between Syn and Syph, I hypothesized that their interaction was due to electrostatic interactions between negatively charged C–terminal region (Ct) of Syph (pI=3.91, charge at pH 7.4 = −4.1) and positively charged Ct of Syn (pI=12.02, charge at pH 7.4 = +19.9), but the exact nature of the mechanism underlying their coacervation remains to be determined.

The Syph Ct is 90 amino acids long and contains evolutionarily conserved 10 repeated sequences, 9 of which start with tyrosine (Y-G-P/Q-Q-G) (6). Interactions among aromatic amino acids such as tyrosine and basic residues such as arginine are known to play a role in phase separation by providing *pi*-cation interactions (7-9). The electron-rich *pi* system above and below the benzene ring is partially negative and this negatively charged region of the quadrupole interacts with positively charged amino acids (10). Besides, *pi*-*pi* stacking interactions among the aromatic rings can also drive LLPS (8, 11). Glycine, proline, and glutamine, collectively known as "disorder-promoting amino acids" (12-14), are also abundant in the Syph Ct. These suggest that Syph Ct may have a propensity for phase separation by mediating networks of interactions either with itself or with other proteins via *pi*-mediated interactions.

Here I found that the coacervation between Syph and Syn is primarily governed by multivalent *pi*-cation electrostatic interactions among tyrosine residues of Syph Ct and positively charged Syn. I showed that Syph Ct can undergo LLPS via *pi*-*pi* interactions between themselves but only when incubated at non-physiologically high concentrations *in vitro* or when assisted by additional interactions in living cells. I further showed that mutating 9 tyrosine residues to serine (9YS) in the repeated sequences of Syph Ct completely abolished the phase-separating property of Syph Ct. Accordingly, Syph Ct 9YS mutant failed to phase-separated with Syn despite this mutant retaining the negative charge of Syph, indicating that electrostatic *pi*-cation interactions rather than simple negative-positive charge interactions mainly govern the coacervation between them. Together with previous results of our group, current findings

further showed that a minimal reconstitution system in fibroblast can be a powerful model to gain mechanistic insight into the assembly of presynaptic structures. My results further raise the possibility that modulation of *pi*–cation interactions between Syph and Syn by interactions with various presynaptic proteins during synaptic activity may control the dynamics of synaptic vesicle clustering.

Materials and Methods

Plasmid DNA construction

The mouse synaptophysin-EGFP (Syph-EGFP) plasmid was kindly provided by Dr. Jane Sullivan (University of Washington, Seattle, WA). The synaptophysin C-terminal (Syph Ct, amino acids 219-308) was PCR-amplified and cloned into mCherry-N1. pCRY2PHR-mCherryN1 (Addgene plasmid # 26866) was a gift from Dr. Chandra Tucker. Syph Ct-mCh-CRY2PHR was made by amplifying CRY2PHR (amino acids 1-498) and cloning into Syph Ct-mCherry. pCMV-CIB1-mCerulean-MP was a gift from Dr. Won Do Heo (Addgene plasmid # 58366), and CIB1 was replaced with Syph Ct to construct Syph Ct-mCer-MP. To make Syph $(Ct)_2$-mCer-MP, the Syph Ct sequence followed by a flexible linker sequence (amino acid sequence: GSAGSAAGSGEF) was inserted before the Syph Ct-mCer-MP sequence. To construct Syph Ct-linker-mCer-MP, the 90 amino acids-long linker from human NHE6 (amino acids 628-701) was PCR-amplified and inserted between Syph Ct and mCer of Syph Ct-mCer-MP sequence. Syph 9YS-HA was derived from Syph-HA by conducting multiple rounds of site-directed mutagenesis in 9 tyrosine residues in Syph Ct (Y245S, Y250S, Y257S, Y263S, Y269S, Y273S, Y284S, Y290S, and Y295S) with custom-made primers (Macrogen, Seoul, South Korea) using *i*-pfu (iNtRON Biotechnology, Seoul, South Korea). Syph Ct 9YS was PCR-amplified and replaced Syph Ct of Syph Ct-mCh-CRY2PHR to construct Syph Ct 9YS-mCh-CRY2PHR. Syph $(Ct)_2$ 9YS-mCer-MP was derived from Syph $(Ct)_2$-mCer-MP by 9YS mutations as

described above. FUS-RBD (amino acids 212-500) was PCR-amplified from the full-length FUS (Korea Human Gene Bank, South Korea) and subcloned into mEGFP-N1. The mCherry-synapsin Ia (mCh-Syn) plasmid was provided by Dr. Roger Tsien, (University of California, San Diego). Syph Ct from Syph Ct-mCherry was subcloned into a pSNAPf vector (N9183S, NEB). Syph Ct-mCh, Syph Ct 9YS-mCh, Syph $(Ct)_2$-mCer-MP, Syph $(Ct)_2$ 9YS-mCer-MP, SNAP-Syph Ct, and FUS-RBD-mEGFP were subcloned in pET28a vector having N-terminal hexahistidine (6xHis) tag to purify proteins. The fidelity of all DNA constructs was validated by DNA sequencing.

Antibodies

Primary antibodies; anti-HA (MMS-101R, Covance, Princeton, NJ), and anti-mCherry (ab167453, Abcam, Cambridge, MA, USA). Secondary antibodies; Goat anti-mouse IgG (H+L) Cross-adsorbed secondary antibody, Alexa Fluor 488 (A-11001, Invitrogen, Carlsbad, CA, USA), and Goat anti-rabbit IgG (H+L) cross-adsorbed secondary antibody, Alexa Fluor 568 (A-11011, Invitrogen).

Cell culture and transfection

COS-7 cells were grown in Dulbecco's modified eagle medium (DMEM, Welgene, Seoul, South Korea) with 10% fetal bovine serum (FBS, Gibco, Carlsbad, MD, USA), and 1% penicillin and streptomycin (Corning, Corning, NY, USA) in a 37℃, 5% CO_2 humid incubator. For transfection, PEI Max (Polyscience, Warrington, PA, USA) was mixed with plasmid DNAs in a 1:4 ratio (w/v) and the mixture was incubated for 20 min at room temperature (RT). The culture medium

was replaced with serum-free DMEM and the mixture was added to the cells and incubated for 3 h at 37℃ in a CO_2 incubator. After incubation, the medium was replaced with a fresh complete medium.

Fluorescence imaging

All live-cell imaging except fluorescence recovery after photobleaching (FRAP) was performed using a 60X oil immersion objective lens (Plan Apo NA 1.4) on a Nikon spinning disk confocal microscope (CSU-X1, Nikon, Tokyo, Japan) equipped with a Neo sCMOS camera (Andor Technology, Belfast, Ireland). During imaging, cells were incubated in Tyrode's solution (136 mM NaCl, 2.5 mM KCl, 2 mM $CaCl_2$, 1.3 mM $MgCl_2$, 10 mM HEPES, and 10 mM glucose, pH 7.3).

Light-activated CRY2PHR clusters formation: For CRY2PHR activation, 500 ms pulses of photoexcitation were delivered 5 times with a 488 nm laser using the photo-stimulation module in the Nikon imaging software (NIS-elements), and a 560 nm laser was used for mCherry imaging. The 488 nm laser setting in our spinning disk confocal microscope, corresponding to ~200 μW (measured with optical power meter 8230, ADCMT, Saitama, Japan), is sufficient to drive rapid phase separation of CRY2PHR-tagged Syph.

1,6-Hexanediol (1,6-HD) treatment: COS-7 cells transfected Syph $(Ct)_2$-mCer-MP were imaged every 2 s using a 405 nm laser. After acquiring the first five images, 3% 1,6-Hexanediol (240117, Sigma) was added to the cells for 1 min and washed.

Fluorescence recovery after photobleaching (FRAP): Photobleaching was performed using Nikon A1 confocal microscope (Nikon) with a

60X oil immersion lens (1.40 N.A.) and Nikon imaging software (NIS-elements). Time-lapse images were acquired every 1 s during 5 s, and a selected droplet was bleached with a 405 nm laser (100%) for 1 s. Fluorescence recovery was subsequently imaged every 1 s during the first 30 s and then every 2 s for 2.5 min. Fluorescence intensity in the bleached region was measured over time, normalized to the initial value, and plotted using Prism 8 (GraphPad Software, San Diego, CA, USA).

Immunocytochemistry (ICC)

Transfected COS-7 cells were washed several times using pre-warmed Tyrode's solution and fixed in a 4% paraformaldehyde (PFA) with 4% sucrose for 15 min at RT and washed with phosphate buffered saline (PBS). The cells were permeabilized with 0.25% Triton X-100 in PBS for 5 min at RT and blocked with 10% bovine serum albumin (BSA) for 30 min at 37℃. Then, cells were incubated with primary antibodies diluted (1:1500) in 3% BSA in PBS at 4℃ overnight. The cells were washed with PBS 3 times and incubated with Alexa Fluor-conjugated secondary antibodies (1:2000) in 3% BSA in PBS for 45 min at 37℃.

Protein purification

All proteins were expressed in *Escherichia coli* BL21 (DE3). Cells were grown at 37℃ in 2xYT medium with kanamycin (50 μg/ml) to A_{600} 0.6-0.8, followed by induction with 0.5 mM isopropyl-β-D-thiogalactopyranoside (IPTG) for 4 h at 37℃ or overnight at 16℃. The cell pellet was collected by centrifugation and resuspended in a lysis buffer (50 mM NaH_2PO_4 (pH 8.0), 300 mM NaCl, 10 mM imidazole, 1 mg/ml lysozyme, 0.1 mg/ml DNase I, protease inhibitor

cocktail (including 104 μM AEBSF, 80 nM Aprotinin, 4 μM Bestatin, 1.4 μM E-64, 2 μM Leupeptin and 1.5 μM Pepstatin A) (Roche, Mannheim, Germany)) in an ice bath. Resuspended cells were sonicated and rocked for 1 h at 4℃ with 0.5% n-lauroylsarcosine sodium salt. In the case of 6xHis-Syph $(Ct)_2$-mCer-MP, cells were lysed using B-PER (ThermoFisher, Waltham, MA, USA), and proteins were purified using inclusion body solubilization reagent (ThermoFisher). After centrifugation, the supernatant was incubated with Ni-NTA chelating agarose beads (Incospharm, Daejeon, South Korea) at 4℃. Proteins were eluted with a buffer containing 50 mM NaH_2PO_4 (pH 8.0), 300 mM NaCl, 250 mM imidazole. All proteins were quantified by SDS-PAGE and stored at -80℃.

In vitro droplet imaging

The target concentration of protein was reached by mixing the purified proteins diluted with the elution buffer with proper polyethylene glycol 8000 (PEG8000) solutions. The protein mixtures were incubated for 5 min on ice before being placed in the chamber. Protein samples were injected into custom chambers assembled by attaching washed 18 mm coverslips to glass slides with double-sided tape. SNAP-Syph Ct was diluted in the elution buffer with proper PEG8000 and 2 mM dithiothreitol (DTT, D9163, Sigma). Then, SNAP-Cell 505-Star or SNAP-Cell TMR-Star (NEB) was added to reach 40 μM final SNAP ligand concentration. *In vitro* droplets imaging was performed at RT using a 60X oil immersion objective (Plan Apo NA 1.4) on a Nikon spinning disk confocal microscope with 488 nm and 561 nm lasers for mEGFP and mCherry-tagged protein, respectively. Phase separation was confirmed by visual inspection and analysis using ImageJ software (NIH). Particles with a size less

than 0.4 μm^2 and circularity less than 0.8 were excluded.

Results

Syph Ct contains repeated regions and forms liquid droplets alone when incubated at high concentrations *in vitro.*

Our group has recently reported that unlike purified Syn, which can assemble into liquid droplets by phase separation *in vitro*, Syn alone has a diffuse cytosolic distribution when expressed in fibroblasts. Only when Syn is expressed together with Syph, they formed liquid droplets which trap small microvesicles into clusters in living cells (1). Our group further demonstrated the importance of electrostatic charge interactions between them since the increase in the ionic strength of the buffer dissociated Syph Ct from Syn. Our group, however, found no evidence of physical interaction between them, and thus the underlying mechanism for their coacervation remains to be determined.

Syph Ct contains 10 repeated regions, 9 of which start with tyrosine (6) **(Figure 1a, b)**. Besides 9 tyrosine residues, glycine is the most frequently occurring amino acid (25/91) **(Figure 1c)**. Glycine-rich regions are known as optimal spacers because they render conformational flexibility of the peptide bonds. Proline and glutamine are the next abundant amino acids (13 and 12/91) **(Figure 1c)**. Proline acts as a structural disruptor of regular secondary structures and is known as the most disorder-promoting residue (14). The glutamine residue, also known as a disorder-promoting residue, is required for the formation of labile cross-beta sheets (12). Therefore, Syph Ct has a high propensity for phase separation

and is indeed predicted to be an IDR (Figure 1d).

I previously showed that purified Syph Ct at 5 μM alone failed to form liquid droplets even in the presence of a crowding agent, PEG (1). I have now found that further increasing the concentration of Syph Ct-mCherry to 50 μM (Figure 2a) resulted in the formation of liquid droplets, indicating that Syph Ct can undergo LLPS *in vitro* although at non-physiologically high concentration. I also found that SNAP-tagged Syph Ct formed liquid droplets *in vitro* in the presence of PEG (Figure 3).

When Syph Ct-mCherry was expressed in COS-7 cells, however, it did not form liquid droplets (Figure 2b) even with extended expression times. This does not rule out phase-separating properties of Syph Ct, as other proteins, for example, synapsin undergoes phase separation only when incubated alone in a physiological buffer rather than in the cytoplasm of living cells.

Syph Ct undergoes phase separation among itself when assisted by additional interactions in living cells.

Whether a system undergoes phase separation depends strongly on the local concentration of macromolecules (8). I reasoned that the failure to form droplets in living cells could be due to the fact that the local concentration of Syph Ct by transient transfection did not reach the threshold concentration, the concentration above which the system starts to phase separate.

To determine whether Syph Ct could self-assemble in living cells if its local concentration increases, I employed the Opto-droplet system developed by the Brangwynne group (15). In this system, the protein of interest is fused to CRY2PHR, which undergoes clustering in response to blue light but does not form droplets on its own. However, if the protein moiety fused to CRY2PHR has the propensity to self-assemble by phase separation, these clusters become nucleation sites for liquid droplet formation when light induces clustering of the fusion protein (15).

I generated a chimeric protein consisting of Syph Ct, CRY2PHR, and mCherry (Syph Ct-mCh-CRY2PHR) and transfected it in COS-7 cells **(Figure 4a)**. Syph Ct-mCh-CRY2PHR showed diffuse cytosolic distribution in the dark but formed distinct droplets when briefly stimulated with blue light for 500 ms. Longer stimulation produced larger Syph Ct-mCh-CRY2PHR droplets **(Figure 4b)**, which remained after cessation of illumination. In contrast, CRY2PHR alone failed to form droplets even with extended stimulation for 2,500 ms **(Figure 4c)**, indicating that CRY2PHR serves only as a nucleating mediator.

Syph is known to assemble into hexamers on the SV membrane and since ~30 copies of Syph are present in each SV, each SV contains 5-6 such hexamers (16-18). To mimic such a high copy number of Syph in non-neuronal systems, I utilized the property of the C-terminal region of Ca^{2+}/Calmodulin-dependent kinase IIα (CaMKIIα) that self-assembles into a circular oligomer of 12 identical subunits (called MP, a multimeric protein) (19). Such oligomer has an outer diameter of about 30 nm, which well matches the average diameter of SVs (39.5 nm).

I first generated a Syph Ct-mCer-MP construct in which a Syph Ct was tagged to each MP subunit, and a circular oligomer contained 12 copies of Syph Ct. However, it failed to form liquid droplets when expressed in COS-7 cells **(Figure 5a)**.

I next generated a Syph $(Ct)_2$-mCer-MP in which each mCer-MP was fused to two Syph Cts linked by a short linker and, thus a circular oligomer contained 24 copies of the Syph Ct **(Figure 6a)**. I found that it readily formed droplets in COS-7 cells **(Figure 6b)**. Simply increasing the length by inserting a linker (90 amino acids long, the same length as Syph Ct) between Syph Ct and MP failed to induce droplet formation **(Figure 5b)**. Purified Syph $(Ct)_2$-mCer-MP also underwent phase separation in the presence (at 5 μM concentration **(Figure 6c)** or absence at 25 μM concentration **(Figure 7)** of PEG at physiological salt concentration.

The liquid nature of Syph $(Ct)_2$-mCer-MP droplets was confirmed by their property to coalesce into larger droplets **(Figure 8a)** and also by 1,6-Hexanediol (1,6-HD) treatment, aliphatic

alcohol that disrupts weak hydrophobic interactions and dissolves LLPS droplets (20, 21). I found that Syph $(Ct)_2$−mCer−MP droplets dissolved within seconds after 3% 1,6−HD treatment and reformed rapidly upon 1,6−HD removal **(Figure 8b)**. Additionally, the FRAP experiment showed that the fluorescence of Syph $(Ct)_2$−mCer−MP droplets recovered rapidly after cessation of photobleaching **(Figure 8c, d)**, indicating the dynamic exchange of Syph $(Ct)_2$−mCer−MP with those in the surrounding cytoplasm.

Phase separation of Syph Ct alone is driven by tyrosine–tyrosine interactions

Syph Ct contains 9 tyrosine residues and multiple disorder-promoting residues. *Pi–pi* stacking interactions between the aromatic rings of tyrosine are known to drive phase separation (8, 11). Indeed, I found that the PScore, a predictive score of the propensity of *pi–pi* interaction of a protein (11) of Syph Ct was 5.147 on average, which is higher than the confidence threshold **(Figure 9)**. Therefore, I reasoned that tyrosine residues in Syph Ct are likely involved in self-interacting networks that lead Syph Ct to phase separation.

To test this possibility, I generated 9YS CRY2PHR and MP mutants in which all nine tyrosine residues (Y245, Y250, Y257, Y263, Y269, Y273, Y284, Y290, and Y295) were replaced with serine **(Figure 10a)**. I found that when expressed in COS-7 cells, Syph Ct 9YS-mCh-CRY2PHR did not form any droplets even with extended light stimulation **(Figure 10b)**. Likewise, Syph $(Ct)_2$ 9YS-mCer-MP failed to form droplets in COS-7 cells **(Figure 10c)** as well as *in vitro* **(Figure 10d)**. These findings are consistent with the possibility that phase separation of Syph Ct alone is mediated by *pi*-stacking interactions among tyrosine residues.

Multivalent *pi*–cation electrostatic interactions tune the coacervate behavior between Syph and Syn.

Purified Syph Ct could be forced to phase separate *in vitro* at a non–physiologically high concentration (50 μM) in the presence of PEG **(Figure 2a)**. However, Syph Ct alone was able to phase separate only when tagged with CRY2PHR or multimeric proteins in living cells **(Figure 4–8)**. These results suggest that phase separation of Syph Ct alone by *pi–pi* stacking may require a significant number of Syph Cts confined in very close proximity. In contrast, I hypothesized that *pi*–cation electrostatic attractions between tyrosine residues in Syph Ct and positively charged amino acids in other proteins could facilitate coacervation between them.

To gain support to this hypothesis, I first co–expressed Syph Ct with Fused in sarcoma RNA binding domain (FUS–RBD). The major determinant of FUS–induced LLPS is known as the intermolecular *pi*–cation interactions between tyrosine residues in its prion–like domain (PLD) and multiple arginine residues in its RBD (8). Thus, I used a FUS–RBD as a surrogate provider of positive arginine residues, expecting it to interact with tyrosine residues in Syph Ct via *pi*–cation interactions. I found that purified 5 μM Syph Ct and 2.5 μM FUS–RBD mixed at a physiological salt concentration in the presence of PEG readily formed co–condensates *in vitro* **(Figure 11a)**, suggesting that tyrosine residues in Syph Ct can mediate *pi*–cation interactions with positively charged residues, leading to phase separation at a much lower concentration than Syph Ct alone (50 μM, **Figure 2a**). This is consistent with my previous results that 5 μM Syph Ct readily forms co–condensate *in vitro* in the presence of PEG when mixed with Syn (1), indicating that the

threshold concentration necessary to drive phase separation based solely on tyrosine residue-based interaction alone is at least an order of magnitude higher than that of tyrosine-basic residue-based interactions (50 μM vs. 5 μM).

Syn contains 85 positively charged amino acids and also has a polybasic C-terminal IDR that contains 31 positively charged residues, most of which are arginine (21/31) (1, 22). To determine whether tyrosine residues in Syph Ct are critical for the coacervation between Syph and Syn, I co-expressed mCh-Syn with Syph-HA or Syph 9YS-HA in COS-7 cells. I found that while Syph-HA phase-separated with mCh-Syn, which is consistent with my previous results (1), Syph 9YS-HA failed to phase-separate with mCh-Syn **(Figure 11b)**. Since I showed that tyrosine residues in Syph Ct can mediate *pi*-cation interactions with positively charged residues, and 9YS mutation retains the negative charge of Syph (-8.3), these results are consistent with the possibility that multivalent electrostatic *pi*-cation interactions rather than simple negative-positive charge interactions mainly govern the coacervation between Syph and Syn in living cells.

Figures

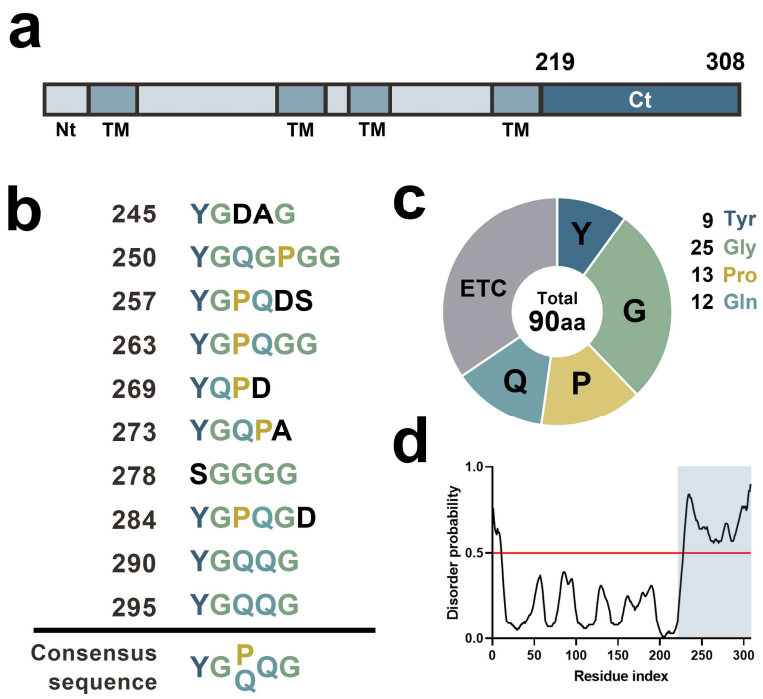

Figure 1. Syph Ct contains repeated regions and is indeed predicted to be an IDR.

(a) Domain structure of full-length mouse Syph. Nt, N-terminus; TM, transmembrane domain; Ct, C-terminus (amino acids 219-308). **(b)** The repeated sequence in the cytoplasmic domain synaptophysin Ct. Syph Ct contains 10 repeated regions, 9 of which start with tyrosine. The repeated sequences are aligned to show the consensus sequence Y-G-P/Q-Q-G. **(c)** The pie graph shows the proportion of Tyr, Gly, Pro, and Gln residue in the Syph Ct. **(d)** The prediction plot of intrinsically disordered regions in the full-length Syph using PrDOS. The shaded region is Syph Ct, which is likely to be an IDR.

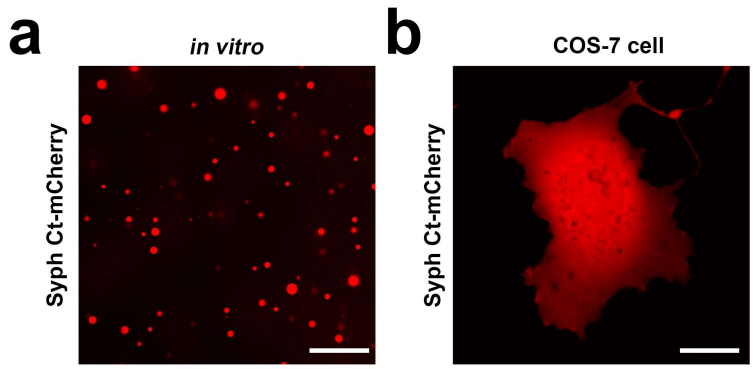

Figure 2. Syph Ct alone forms liquid droplets when incubated at high concentrations *in vitro*.

(a) Fluorescence images showing droplet formation of purified Syph Ct-mCh alone (50 μM) *in vitro* in the presence of 10% PEG8000 at RT. (b) Representative fluorescence image of Syph Ct-mCh expressed in COS-7 cells. Scale bars, 20 μm.

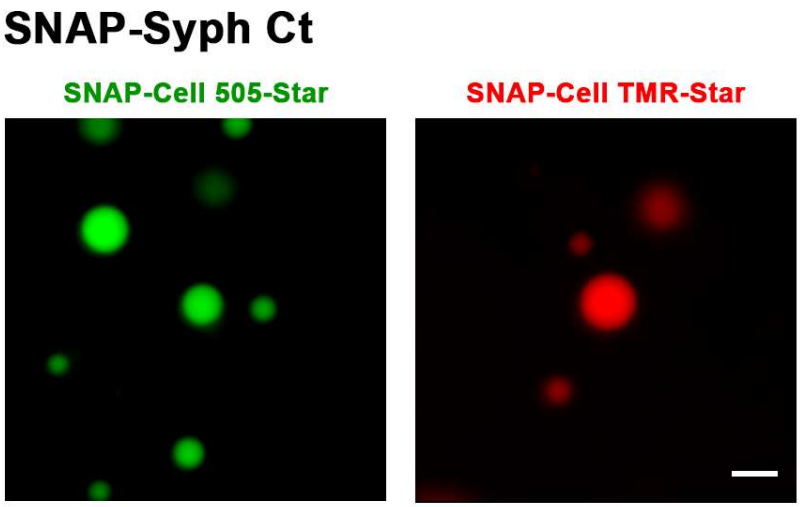

Figure 3. Purified SNAP-Syph Ct forms droplets *in vitro* as shown in Syph Ct-mCherry.

Fluorescence images showing droplet formation of purified SNAP-Syph Ct (40 μM) *in vitro* in the presence of 10% PEG8000 at RT. The SNAP-Syph Ct protein was stained SNAP-ligands, SNAP-Cell 505-Star, or SNAP-Cell TMR-Star. Scale bar, 5 μm.

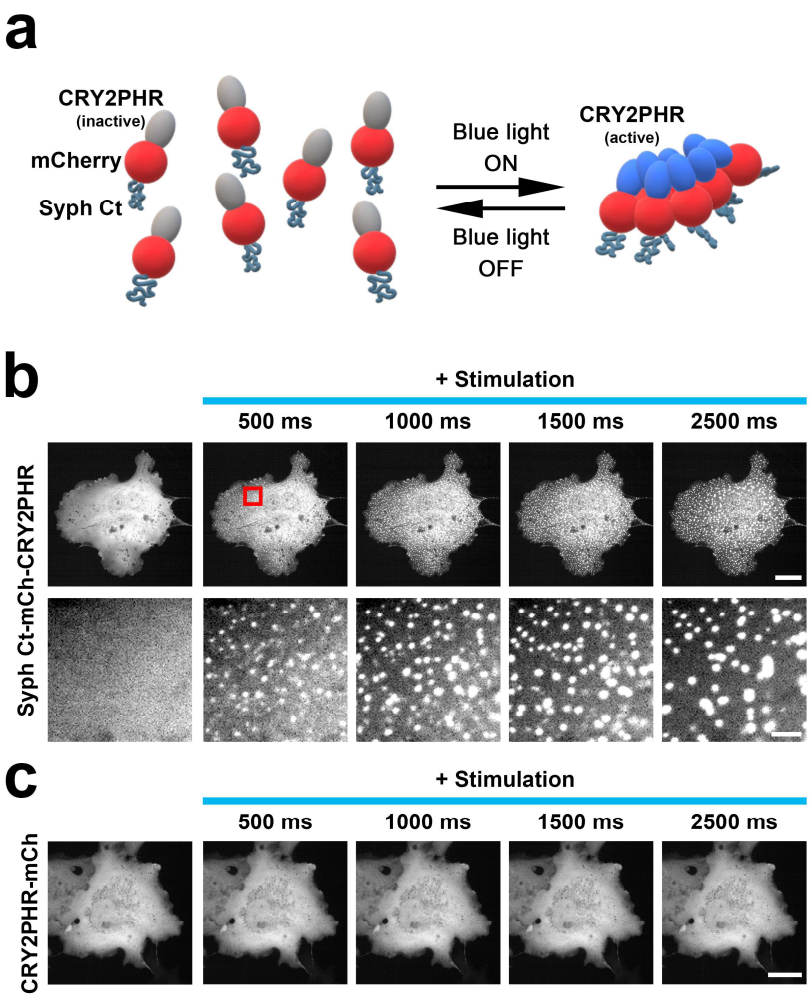

Figure 4. Syph Ct undergoes phase separation among themselves when assisted by the opto-droplet system for additional interactions in living cells.

(a) Schematic diagram of Syph Ct-mCh-CRY2PHR consisting of the N-terminal Syph Ct (blue-gray) fused to mCherry (red) and the CRY2PHR domain (gray indicating inactive state). Blue light activation of Syph Ct-mCh-CRY2PHR leads to rapid clustering (blue indicating active CRY2PHR). (b) Representative time-lapse

fluorescence images of light-activated clustering of Syph Ct-mCh-CRY2PHR stimulated with a 488 nm laser for 2,500 ms. Bottom: Magnified images of the region enclosed by a red rectangle in the top panel. (c) Representative time-lapse fluorescence images of light-activated clustering of CRY2PHR-mCh stimulated with a 488 nm laser for 2,500 ms. Scale bars; 20 μm (2b top and 2c), 2 μm (2b bottom).

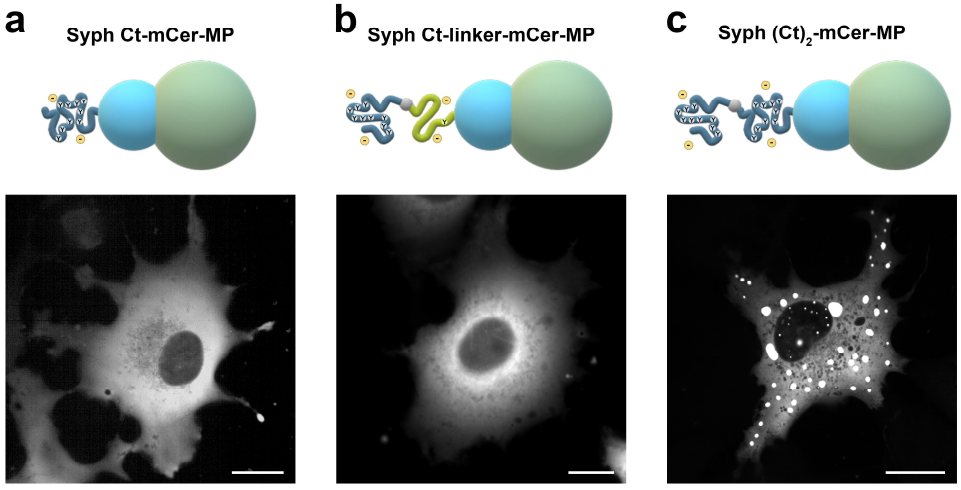

Figure 5. Single Syph Ct tagged to MP or increased length by inserting the linker failed to form droplets in COS-7 cells.

(a-c) Schematic diagrams and fluorescence images of COS-7 cells expressed Syph Ct-mCer-MP (a), Syph Ct-linker-mCer-MP (b), and Syph $(Ct)_2$-mCer-MP (c). Syph Ct-mCer-MP failed to form droplets and increasing the length by inserting the linker (90 amino acids long, the same length as C-term) between C-term and MP also failed to induce droplet formation. Scale bars, 20 μm.

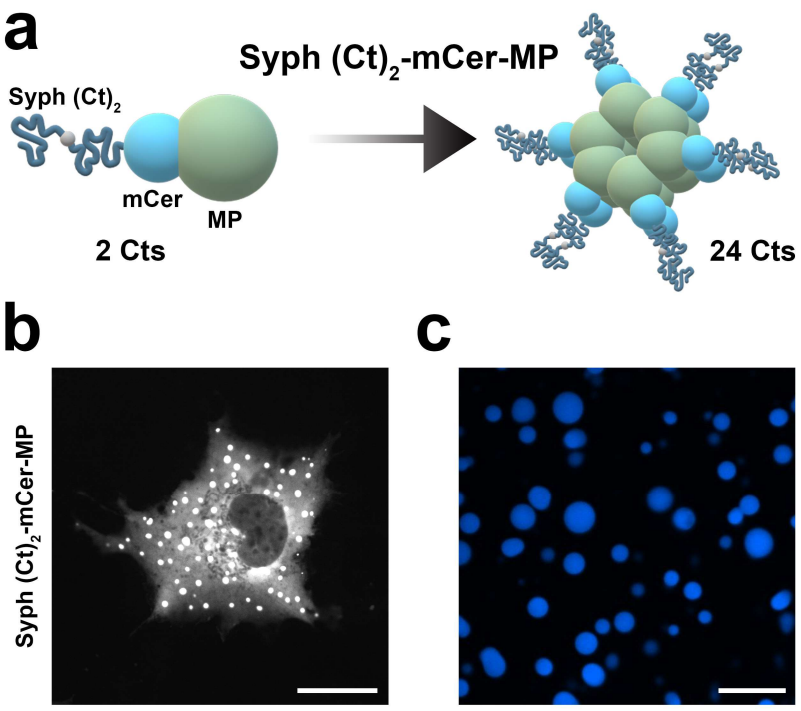

Figure 6. The artificial clustering of multiple Syph Cts by MP tagging induced LLPS of Syph Ct alone in living cells and *in vitro*.

(a) Schematic diagram of Syph $(Ct)_2$−mCer−MP. Two Syph Cts were linked by a short linker (gray) and fused to mCerulean fluorescent protein and the multimeric protein (MP) of CaMKIIα (pale mint). 12 identical MP subunits are assembled into a circular oligomer, exposing 24 copies of Syph Cts. (b) Representative fluorescence image of droplets formed by Syph $(Ct)_2$−mCer−MP expressed in living cells. (c) Representative fluorescence image of droplets formed by purified Syph $(Ct)_2$−mCer−MP (5 μM) *in vitro* in the presence of 3% PEG8000. Scale bars; b=20 μm, c=10 μm.

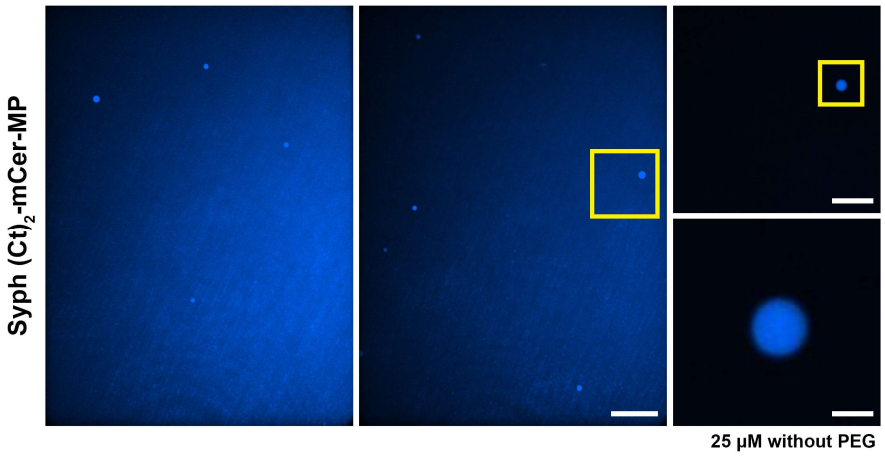

Figure 7. Purified Syph (Ct)$_2$–mCer–MP forms droplets *in vitro* at a high concentration (25 μM) without crowding reagent.

Representative fluorescence images of purified Syph (Ct)$_2$–mCer–MP at a high concentration (25 μM) *in vitro* in the absence of crowding reagent, PEG8000. A series of magnified images of the regions enclosed by yellow rectangles (center → top right → bottom right). Scale bars, center: 20 μm, top right: 10 μm, bottom right: 2 μm.

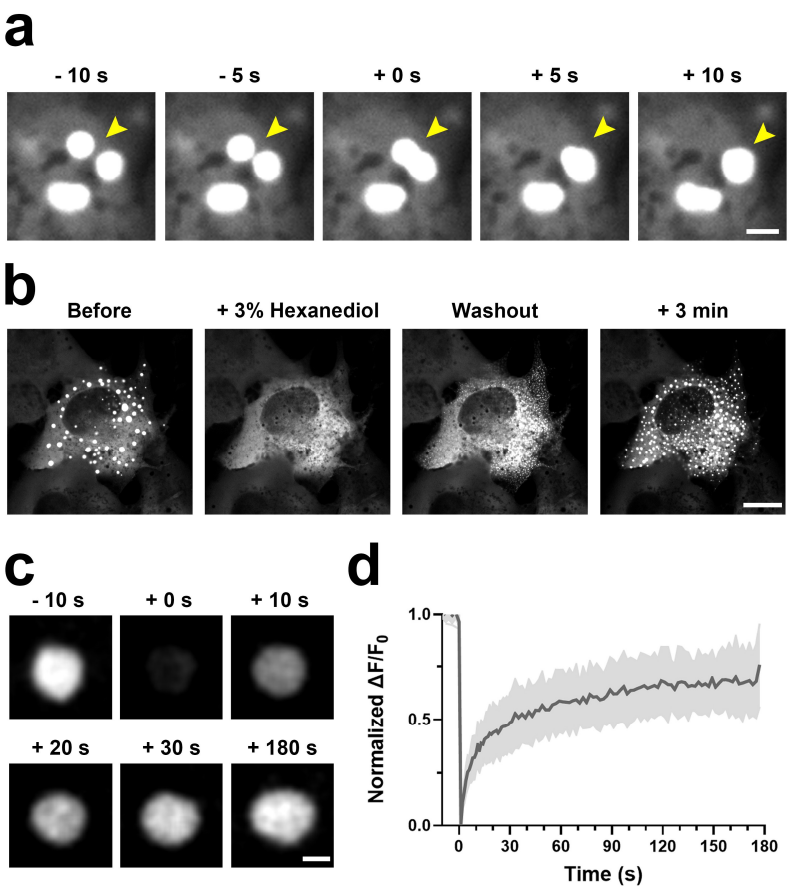

Figure 8. The liquid nature of Syph $(Ct)_2$-mCer-MP droplets was confirmed.

(a) Time-lapse images showed the fusion of two Syph $(Ct)_2$-mCer-MP droplets in living cells. (b) Representative fluorescence images of Syph $(Ct)_2$-mCer-MP droplets treated with 3% 1,6-Hexanediol (3% 1,6-HD). Droplets disperse reversibly upon 3% 1,6-HD. (c) Representative time-lapse images showing fluorescence recovery of Syph $(Ct)_2$-mCer-MP droplet after photobleaching. (d) The plot of the average fluorescence intensities after photobleaching of multiple spots. N=10 cells from 5 coverslips. Scale bars; a and c=2 μm,

b=20 μm.

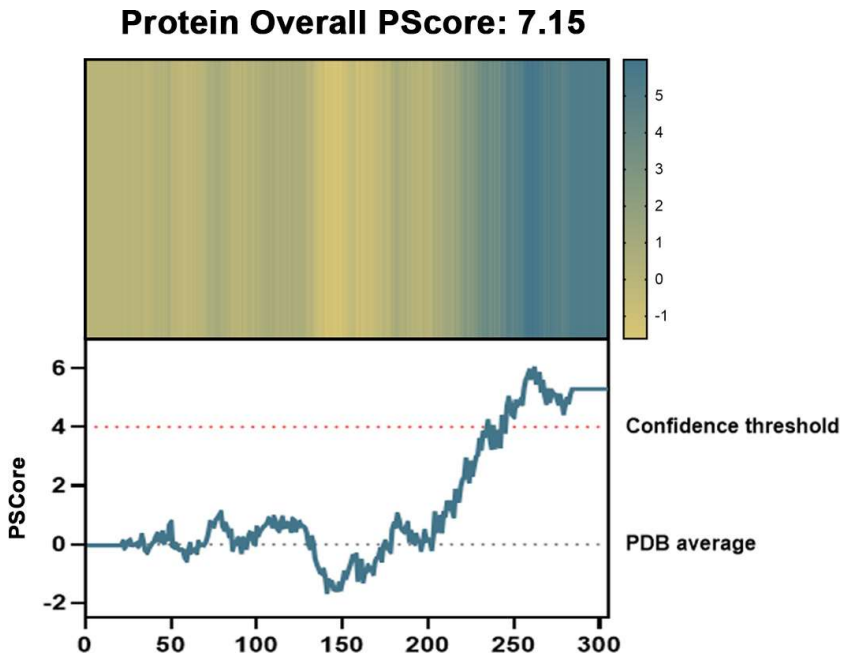

Figure 9. The PScore plots of synaptophysin

Heat map and a line graph of synaptophysin PScore, which is the propensity score of *pi*–*pi* interaction tendency by prediction. X and Y axes are amino acids and PScore, and the average PScore of repeat sequence in Syph Ct is 5.147.

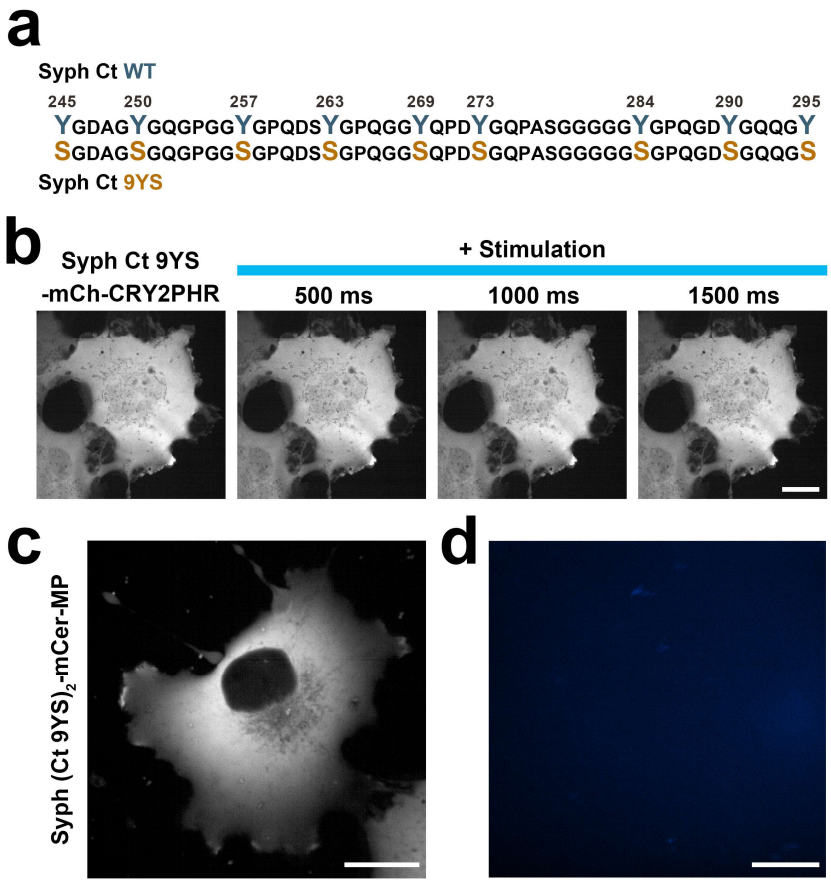

Figure 10. Phase separation of Syph Ct alone is driven by tyrosine–tyrosine interactions.

(a) Schematic diagram of Syph Ct WT and 9YS mutant. Y245, Y250, Y257, Y263, Y269, Y273, Y284, Y290, and Y295 were mutated to serine (9YS). (b) Representative time–lapse fluorescence images of light–activation of Syph Ct 9YS–mCh–CRY2PHR in COS–7 cells. (c, d) Representative fluorescence image of Syph $(Ct)_2$ 9YS–mCer–MP expressed in COS–7 cells (c) and purified Syph $(Ct)_2$ 9YS–mCer–MP at 10 μM *in vitro* in the presence of 3% PEG8000 (d). All scale bars, 20 μm.

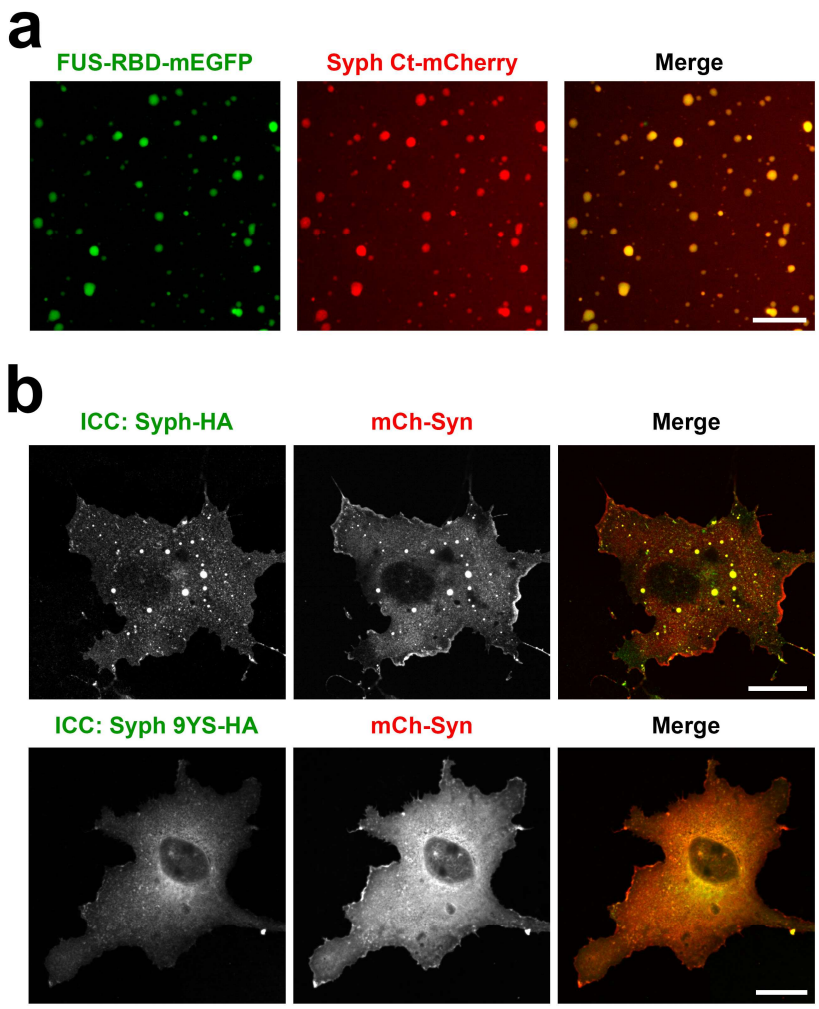

Figure 11. *Pi*–cation electrostatic interactions govern the coacervate behavior between Syph and positively charged proteins.

(a) Representative fluorescence images of co–condensates formed by purified Syph Ct–mCh and FUS–RBD–mEGFP *in vitro*. Syph Ct–mCh (5 μM) and FUS–RBD–mEGFP (2.5 μM) were mixed with 5% PEG8000. (b) COS–7 cells were transfected with Syph–HA and mCh–Syn (top) or Syph 9YS–HA and mCh–Syn (bottom), and Syph was detected by immunocytochemistry staining of HA (ICC). Unlike

Syph-HA, no droplets were observed with Syph 9YS expression. All scale bars, 20 μm.

Discussion

In our previous study, we demonstrated that the presence of Syn and Syph, two presynaptic proteins, in the cytoplasm of non-neuronal cells is capable of triggering the formation of vesicle clusters that bear a striking resemblance to authentic SV clusters in both their physical structure and liquid characteristics (1). Despite the absence of any direct physical interaction between these proteins, the precise mechanism responsible for their coacervation phenomenon remains elusive. Thus, the present investigation aimed to elucidate the underlying mechanism driving the phase separation between Syph and Syn.

The Syph Ct region contains a distinctive pattern of 10 repeated sequences, each consisting of 9 tyrosine residues. Through my investigation, I have observed that these tyrosine residues play a crucial role in facilitating both *pi-pi* interactions among themselves and *pi*-cation interactions with other positively charged proteins. These interactions, occurring both *in vitro* and within living cells, are responsible for the observed phase separation phenomenon. Furthermore, in addition to the 9 tyrosine residues, the Syph Ct region contains a significant presence of glycine, proline, and glutamine amino acids, all known as disorder-promoting residues (12, 14).

The phase behavior of associative polymers is primarily dictated by the interactions between specific motifs known as

"stickers," while the spacers between these stickers play a lesser role in the driving forces behind phase separation (23, 24). Similarly, to the FUS protein (8), in the case of Syph and Syn, the stickers are represented by the tyrosine residues and positively charged residues, while the abundant glycine and proline residues serve as effective spacers, facilitating the induction of phase separation.

Pi-pi interactions are commonly observed in aromatic rings, such as those present in the side chains of tyrosine, phenylalanine, and tryptophan. These interactions occur due to the availability of pi orbitals from the bonded sp^2-hybridized atoms (11, 25). It is worth noting that low complexity intrinsically disordered regions (IDRs) associated with phase separation in proteins like FUS, EWS, hnRNPA1, TIA-1, TDP-43, and the RNA Pol II C-terminal domain (CTD) (26-28) are particularly enriched in these aromatic residues, suggesting a high likelihood of *pi-pi* interactions. Similarly, the Syph Ct region also consists of 9 tyrosine residues. The PScore, which is a predictive score indicating the propensity of a protein for *pi-pi* interactions (11), for the Syph Ct region was found to exceed the confidence threshold **(Figure 9)**.

Indeed, my findings demonstrated that the artificial clustering of multiple Syph Ct regions, either through CRY2PHR-tagging or MP tagging, induced phase separation and LLPS of Syph Ct alone, both *in vitro* and within living cells **(Figure 4-8)**. These results align with our previous discovery that Syph-EGFP, when tagged with EGFP due to EGFP's dimeric nature, readily formed liquid droplets (1). The significance of *pi-pi* interactions involving the tyrosine residues in the Syph Ct region was further supported by my experiments, which

revealed that the phase-separating property of Syph was completely abolished upon the introduction of the 9YS mutation **(Figure 10)**.

Pi-cation interactions refer to noncovalent molecular interactions that occur between electron-rich *pi*-systems and adjacent cations. Recent studies have highlighted the significance of these interactions as a driving force for liquid-liquid phase separation (LLPS) (7, 9, 10). In the case of FUS, for instance, the phase-separating behavior is primarily attributed to *pi*-cation interactions between tyrosine residues in the poly-low complexity domain (PLD) and arginine residues in the RNA-binding domain (RBD) (8, 29). Interestingly, increasing the number of *pi*-cation interactions through arginine substitutions in the FUS protein has been shown to significantly enhance its phase separation ability and lower the concentration threshold for phase transition (8).

In my investigations, I utilized the FUS-RBD as a surrogate provider of positive arginine residues to explore the role of tyrosine residues in the Syph Ct region. The results demonstrated that tyrosine residues in Syph Ct can indeed mediate *pi*-cation interactions with other positively charged proteins, leading to coacervation **(Figure 11a)**. Syn, on the other hand, contains a substantial number of positively charged amino acids (85 in total) and possesses a polybasic C-terminal intrinsically disordered region (pI=12.02) consisting of 31 positively charged residues, primarily arginine (22).

While it was impractical to mutate all positively charged amino acids in Syn, my findings support the following observations: 1)

Tyrosine residues in Syph Ct can facilitate *pi*–cation interactions with positively charged residues; 2) Co–expression of Syph 9YS with Syn completely inhibited the formation of co–condensates, unlike the wild–type Syph **(Figure 11b)**; and 3) The 9YS mutation in Syph retains its negative charge (–8.3). Based on these results, it is plausible to propose that multivalent electrostatic *pi*–cation interactions, rather than simple negative–positive charge interactions, predominantly govern the coacervation between Syph and Syn within living cells.

Several SV proteins are predicted to possess intrinsically disordered regions (IDRs). For instance, Synaptotagmin1 and VAMP2, which are single transmembrane domain proteins, also feature IDRs in their cytoplasmic regions. Notably, VAMP2 interacts with Syph through its cytoplasmic region, forming Syph–VAMP2 heterodimers (30, 31). Interestingly, studies involving Syph knockout (KO) have not revealed any evident abnormalities in synaptic physiology, including SV clustering (32, 33). These findings suggest that the function of Syph may overlap with that of other SV proteins. Consequently, the composition of SV clusters could be dynamically regulated by different LLPS formations facilitated by various presynaptic proteins, depending on the physiological requirements.

Through recent studies, it has been confirmed that LLPS is involved in the SVs clustering in the presynapse and the regulation of the active zone (34). Particularly, the additional condensation of SVs has been proposed early on, as it occurs independently of synapsin within the active zone (35). RIMS1 (regulatory synaptic

membrane exocytosis protein 1), which has been found to be highly disordered in nature, has been shown to perform LLPS (36). While RIMS1 can undergo self-condensation, the presence of RIM-binding proteins (RIMBPs) significantly enhances phase separation. RIMBP2 has been identified as one of the interacting proteins. Furthermore, the condensates of RIM/RIMBP have been observed to form co-condensates with the intracellular C-terminal region of the voltage-dependent N-type calcium channel subunit alpha-1B (CACNA1). Based on these findings, it is possible that these condensates can localize the voltage-gated calcium channels to the site of SV release (36-38).

Disruption of tight tethering and priming of SVs at the active zone is observed in the absence of all RIM/RIMBP proteins, with a quadruple knockout (39). However, overall, the recruitment of a larger pool of SVs to the active zone remains minimally affected. RIM is known to interact with various proteins such as Rab3, Munc13, ELKS, and liprin-alpha (40), implying their potential as partners that contribute additional functionality to RIM/RIMBP condensates, thereby expanding their assembly and support. Notably, Munc13, a crucial protein involved in SV docking and priming during SV exocytosis (41, 42), exhibits a highly disordered structure and carries a strong negative charge within the cytoplasm. Previous studies have reported that Munc13 can form a hexameric "buttressed rings" structure using its MUN domain (43), and it interacts with RIM through the N-terminal C2A domain (44), forming a heterodimeric complex (44). Given the important role of Munc13 and the reported findings, it can be postulated that Munc13 may have a high potential for involvement in both RIM-alone and RIM/RIMBP LLPS

condensates.

Post-translational modifications (PTMs) and phosphorylation of proteins have been recognized as influential factors in the behaviors of LLPS (7, 45-47). Phosphorylation, a rapid and reversible protein modification, can alter intra- and intermolecular electrostatic interactions by modifying the charge distribution within proteins. Notably, phosphorylation status has been shown to affect the LLPS tendencies of proteins such as FUS, TDP-43, and Tau, with FUS and TDP-43 exhibiting decreased LLPS propensity while Tau shows an increased propensity depending on their phosphorylation states (7, 46, 47). Specifically, tyrosine phosphorylation can disrupt *pi*-mediated interactions by introducing negative charges to the proteins.

A previous study reported that the tyrosine phosphorylation of Syph has an impact on synaptic vesicle recycling during synaptic activity (48). Additionally, the phosphorylation of Tyr_{273} within the Syph Ct has been confirmed to play a critical role in the binding and activation of Syph with the tyrosine kinase c-src (49). Syph also forms a complex with Dynamin I (DynI) (50, 51), a GTPase essential for synaptic vesicle endocytosis, which can be regulated by the phosphorylation of Syph (49).

Given these findings, it is imperative to investigate the occurrence of LLPS between Syph and DynI, along with the phosphorylation of Syph Ct and tyrosine residues within it, and their impact on the LLPS process between Syph and DynI, as well as their potential influence on physiological phenomena like endocytosis.

Thus, the question of whether the phosphorylation of tyrosine residues in the Syph Ct region modifies the induction of LLPS by modulating electrostatic interactions with other proteins remains an open inquiry that warrants future studies. Moreover, exploring the physiological significance of these alterations is of great importance.

In addition to protein phosphorylation, methylation occurs on specific amino acids, including arginine (Arg), lysine (Lys), threonine (Thr), and tyrosine (Tyr). This PTMs process is facilitated by specific methyltransferase enzymes, which regulate the addition of methyl groups to target amino acids. Methylation events have been shown to exert significant effects on the structure and functionality of proteins. Notably, the C-terminal region of synapsin encompasses 31 positively charged residues, among which 21 possess the potential for arginine methylation. Extensive investigations have identified Synapsin I as a key endogenous substrate for protein L-Isoaspartyl Methyltransferase in mammalian brain tissues (52). FUS possesses the RGG/RG motif in RBD known to be methylated by protein arginine methyltransferase 1 (PRMT1) (53). It has been reported that methylation of FUS by PRMT1 weakens the *pi*-cation interactions (54). Taking these facts into consideration, it is worth exploring the potential impact of arginine methylation induced by physiological demands on LLPS of synapsin itself or the LLPS involving Syph.

Although the reconstitution system employed in COS-7 cells may not entirely replicate the phenomena observed at presynaptic terminals, and I cannot ascertain the exact impact of the Syph-Syn interaction on SV clustering in living neurons, the present study, in conjunction with our previous work, highlights the utility of a minimal

reconstitution system as a potent tool for investigating the mechanisms underlying the co-assembly of these two presynaptic proteins. Such investigations would otherwise be intricate or obscured by the complex interactions among various presynaptic proteins.

Undoubtedly, interactions involving other synaptic proteins could potentially influence or modulate the *pi*-cation interaction between Syph and Syn. Given that *pi*-cation interactions primarily rely on the interplay between tyrosine and positively charged amino acids, they are susceptible to physiological modifications such as phosphorylation, changes in pH, and protein interactions. Consequently, I hypothesize that physiological modulation of *pi*-cation interactions between Syph and Syn during synaptic activity may contribute to the dynamics of synaptic vesicle clustering.

It is important to note that even in neuronal synapses, the precise stoichiometry governing the interaction between Syph and other proteins, including Syn, remains unknown. Furthermore, despite previous findings (16), whether Syph forms actual hexamers within synaptic vesicles and the significance of this formation for its physiological role are still unresolved questions. Therefore, I am still far from fully comprehending the intricacies of real synapses, necessitating extensive further research.

In this context, I firmly believe that the results obtained from my previous and current studies utilizing the minimal reconstitution system can offer valuable insights into the possible scenarios that may occur at real synapses. These findings are expected to serve as

catalysts for future studies conducted in more physiologically relevant environments, propelling our understanding of synaptic function to new horizons.

References

1. Park, D., et al., *Cooperative function of synaptophysin and synapsin in the generation of synaptic vesicle-like clusters in non-neuronal cells.* Nat Commun, 2021. **12**(1): p. 263.
2. Milovanovic, D., et al., *A liquid phase of synapsin and lipid vesicles.* Science, 2018. **361**(6402): p. 604-607.
3. Hyman, A.A., C.A. Weber, and F. Julicher, *Liquid-liquid phase separation in biology.* Annu Rev Cell Dev Biol, 2014. **30**: p. 39-58.
4. Li, P., et al., *Phase transitions in the assembly of multivalent signalling proteins.* Nature, 2012. **483**(7389): p. 336-40.
5. Boeynaems, S., et al., *Protein Phase Separation: A New Phase in Cell Biology.* Trends Cell Biol, 2018. **28**(6): p. 420-435.
6. Sudhof, T.C., et al., *A synaptic vesicle protein with a novel cytoplasmic domain and four transmembrane regions.* Science, 1987. **238**(4830): p. 1142-4.
7. Lin, Y., S.L. Currie, and M.K. Rosen, *Intrinsically disordered sequences enable modulation of protein phase separation through distributed tyrosine motifs.* J Biol Chem, 2017. **292**(46): p. 19110-19120.
8. Wang, J., et al., *A Molecular Grammar Governing the Driving Forces for Phase Separation of Prion-like RNA Binding Proteins.* Cell, 2018. **174**(3): p. 688-699 e16.
9. Nott, T.J., et al., *Phase transition of a disordered nuage pr*

otein generates environmentally responsive membraneless organelles. Mol Cell, 2015. **57**(5): p. 936-947.

10. Marshall, M.S., et al., *Potential energy curves for cation-pi interactions: off-axis configurations are also attractive.* J Phys Chem A, 2009. **113**(48): p. 13628-32.
11. Vernon, R.M., et al., *Pi-Pi contacts are an overlooked protein feature relevant to phase separation.* Elife, 2018. **7**.
12. Campen, A., et al., *TOP-IDP-scale: a new amino acid scale measuring propensity for intrinsic disorder.* Protein Pept Lett, 2008. **15**(9): p. 956-63.
13. Romero, P., et al., *Sequence complexity of disordered protein.* Proteins, 2001. **42**(1): p. 38-48.
14. Theillet, F.X., et al., *The alphabet of intrinsic disorder: I. Act like a Pro: On the abundance and roles of proline residues in intrinsically disordered proteins.* Intrinsically Disord Proteins, 2013. **1**(1): p. e24360.
15. Shin, Y., et al., *Spatiotemporal Control of Intracellular Phase Transitions Using Light-Activated optoDroplets.* Cell, 2017. **168**(1-2): p. 159-171 e14.
16. Arthur, C.P. and M.H. Stowell, *Structure of synaptophysin: a hexameric MARVEL-domain channel protein.* Structure, 2007. **15**(6): p. 707-14.
17. Takamori, S., et al., *Molecular anatomy of a trafficking organelle.* Cell, 2006. **127**(4): p. 831-46.
18. Wilhelm, B.G., et al., *Composition of isolated synaptic boutons reveals the amounts of vesicle trafficking proteins.* Science, 2014. **344**(6187): p. 1023-8.
19. Bayer, K.U. and H. Schulman, *CaM Kinase: Still Inspiring at 40.* Neuron, 2019. **103**(3): p. 380-394.

20. Kato, M. and S.L. McKnight, *A Solid-State Conceptualization of Information Transfer from Gene to Message to Protein.* Annu Rev Biochem, 2018. **87**: p. 351-390.
21. Lin, Y., et al., *Toxic PR Poly-Dipeptides Encoded by the C9orf72 Repeat Expansion Target LC Domain Polymers.* Cell, 2016. **167**(3): p. 789-802 e12.
22. Ueda, T. and P. Greengard, *Adenosine 3':5'-monophosphate-regulated phosphoprotein system of neuronal membranes. I. Solubilization, purification, and some properties of an endogenous phosphoprotein.* J Biol Chem, 1977. **252**(14): p. 5155-63.
23. Choi, J.M., A.S. Holehouse, and R.V. Pappu, *Physical Principles Underlying the Complex Biology of Intracellular Phase Transitions.* Annu Rev Biophys, 2020. **49**: p. 107-133.
24. Semenov, A.N. and M. Rubinstein, *Thermoreversible Gelation in Solutions of Associative Polymers. 1. Statics.* Macromolecules, 1998. **31**(4): p. 1373-1385.
25. Sherrill, C.D., *Energy component analysis of pi interactions.* Acc Chem Res, 2013. **46**(4): p. 1020-8.
26. Mitrea, D.M. and R.W. Kriwacki, *Phase separation in biology; functional organization of a higher order.* Cell Commun Signal, 2016. **14**: p. 1.
27. Taylor, J.P., R.H. Brown, Jr., and D.W. Cleveland, *Decoding ALS: from genes to mechanism.* Nature, 2016. **539**(7628): p. 197-206.
28. Kato, M., et al., *Cell-free formation of RNA granules: low complexity sequence domains form dynamic fibers within hydrogels.* Cell, 2012. **149**(4): p. 753-67.
29. Qamar, S., et al., *FUS Phase Separation Is Modulated by a*

Molecular Chaperone and Methylation of Arginine Cation-π Interactions. Cell, 2018. **173**(3): p. 720-734.e15.

30. Washbourne, P., G. Schiavo, and C. Montecucco, *Vesicle-associated membrane protein-2 (synaptobrevin-2) forms a complex with synaptophysin.* Biochem J, 1995. **305 (Pt 3)** (Pt 3): p. 721-4.
31. Edelmann, L., et al., *Synaptobrevin binding to synaptophysin: a potential mechanism for controlling the exocytotic fusion machine.* EMBO J, 1995. **14**(2): p. 224-31.
32. Eshkind, L.G. and R.E. Leube, *Mice lacking synaptophysin reproduce and form typical synaptic vesicles.* Cell Tissue Res, 1995. **282**(3): p. 423-33.
33. McMahon, H.T., et al., *Synaptophysin, a major synaptic vesicle protein, is not essential for neurotransmitter release.* Proc Natl Acad Sci U S A, 1996. **93**(10): p. 4760-4.
34. Lautenschläger, J., *Protein phase separation hotspots at the presynapse.* Open Biol, 2022. **12**(2): p. 210334.
35. Pieribone, V.A., et al., *Distinct pools of synaptic vesicles in neurotransmitter release.* Nature, 1995. **375**(6531): p. 493-7.
36. Wu, X., et al., *RIM and RIM-BP Form Presynaptic Active-Zone-like Condensates via Phase Separation.* Mol Cell, 2019. **73**(5): p. 971-984 e5.
37. Grauel, M.K., et al., *RIM-binding protein 2 regulates release probability by fine-tuning calcium channel localization at murine hippocampal synapses.* Proc Natl Acad Sci U S A, 2016. **113**(41): p. 11615-11620.
38. Han, Y., et al., *RIM determines Ca(2)+ channel density and vesicle docking at the presynaptic active zone.* Neuron,

2011. **69**(2): p. 304-16.

39. Acuna, C., X. Liu, and T.C. Südhof, *How to Make an Active Zone: Unexpected Universal Functional Redundancy between RIMs and RIM-BPs.* Neuron, 2016. **91**(4): p. 792-807.

40. Sudhof, T.C., *The presynaptic active zone.* Neuron, 2012. **75**(1): p. 11-25.

41. Augustin, I., et al., *Munc13-1 is essential for fusion competence of glutamatergic synaptic vesicles.* Nature, 1999. **400**(6743): p. 457-461.

42. Siksou, L., et al., *A common molecular basis for membrane docking and functional priming of synaptic vesicles.* Eur J Neurosci, 2009. **30**(1): p. 49-56.

43. Rothman, J.E., et al., *Hypothesis - buttressed rings assemble, clamp, and release SNAREpins for synaptic transmission.* FEBS Lett, 2017. **591**(21): p. 3459-3480.

44. Camacho, M., et al., *Heterodimerization of Munc13 C(2)A domain with RIM regulates synaptic vesicle docking and priming.* Nat Commun, 2017. **8**: p. 15293.

45. Hofweber, M. and D. Dormann, *Friend or foe-Post-translational modifications as regulators of phase separation and RNP granule dynamics.* J Biol Chem, 2019. **294**(18): p. 7137-7150.

46. Owen, I. and F. Shewmaker, *The Role of Post-Translational Modifications in the Phase Transitions of Intrinsically Disordered Proteins.* Int J Mol Sci, 2019. **20**(21).

47. Farina, S., et al., *Post-Translational Modifications Modulate Proteinopathies of TDP-43, FUS and hnRNP-A/B in Amyotrophic Lateral Sclerosis.* Front Mol Biosci, 2021. **8**: p.

693325.

48. Evans, G.J. and M.A. Cousin, *Tyrosine phosphorylation of synaptophysin in synaptic vesicle recycling.* Biochem Soc Trans, 2005. **33**(Pt 6): p. 1350-3.

49. Mallozzi, C., et al., *Phosphorylation and nitration of tyrosine residues affect functional properties of Synaptophysin and Dynamin I, two proteins involved in exo-endocytosis of synaptic vesicles.* Biochim Biophys Acta, 2013. **1833**(1): p. 110-21.

50. Daly, C. and E.B. Ziff, *Ca2+-dependent formation of a dynamin-synaptophysin complex: potential role in synaptic vesicle endocytosis.* J Biol Chem, 2002. **277**(11): p. 9010-5.

51. Daly, C., et al., *Synaptophysin regulates clathrin-independent endocytosis of synaptic vesicles.* Proc Natl Acad Sci U S A, 2000. **97**(11): p. 6120-5.

52. Reissner, K.J., et al., *Synapsin I is a major endogenous substrate for protein L-isoaspartyl methyltransferase in mammalian brain.* J Biol Chem, 2006. **281**(13): p. 8389-98.

53. Tradewell, M.L., et al., *Arginine methylation by PRMT1 regulates nuclear-cytoplasmic localization and toxicity of FUS/TLS harbouring ALS-linked mutations.* Hum Mol Genet, 2012. **21**(1): p. 136-49.

54. Qamar, S., et al., *FUS phase separation is modulated by a molecular chaperone and methylation of arginine cation-π interactions.* Cell, 2018. **173**(3): p. 720-734. e15.

Abstract in Korean (국문초록)

최근 연구에서 신경 세포 외의 생체 내에서 synaptophysin (Syph)과 synapsin (Syn) 단백질이 액체-액체 상 분리 (LLPS)라는 과정을 겪어 시냅스 소포(SV) 클러스터와 유사한 작은 시냅스 모양의 미세 소포들이 군집화 될 수 있다는 것을 최근 입증했었다. 흥미로운 점은 Syph와 Syn 사이에 직접적인 물리적 상호작용이 없음에도 불구하고, 이들의 코아세르베이션 (coacervation) 현상 또는 드롭렛 (droplet)과 같은 군집화 형성 메커니즘은 여전히 알려지지 않았다는 것이다.

이번 연구를 통해 Syph와 Syn 사이의 코아세르베이션이 주로 다가 파이 양이온 정전기적 상호작용 (multivalent electrostatic *pi*-cation interaction)에 의해 주도된다는 것을 보여주었다. 이러한 상호작용은 Syph의 C-말단(Ct) 영역에 존재하는 티로신 (tyrosine) 잔기와 Syn의 양전하를 띤 영역과 관련이 있는 것을 확인하였다. Syph의 본질적으로 무질서한 (intrinsically disordered) C-말단 영역인 Syph Ct가 높은 농도로 세포와 유사하게 밀집되어 있는 *in vitro* 조건에서 자체적으로 액체 드롭렛을 형성하는 것을 발견하였다. 게다가, 빛에 민감한 CRY2PHR 또는 다중 단백질의 서브 유닛으로 태깅을 이용한 추가 상호작용의 도움으로 살아있는 세포 내에서 상 분리 현상을 수행하는 것을 확인하였다.

Syph의 C-말단 영역에는 티로신으로 시작하는 9개의 반복된 서열을 포함한 총 10개의 반복된 서열이 있음을 확인하였다. 흥미롭게도, 이러한 9개의 티로신 잔기를 세린으 (serine)로 돌연변이시키면 (Syph 9YS로 지칭됨) Syph Ct의 상분리 능력이 완전히 사라진다는 것을 발견하였다. 이는 티로신으로 매개되는 파이 (*pi*)-상호작용이 이

과정에서 매우 중요한 역할을 한다는 것을 알 수 있었다. 더욱이, 이번 연구 결과는 9YS 돌연변이가 Syph와 Syn 사이의 코아세르베이션을 방지한다는 것을 밝혀내었다. 특히, Syph 9YS는 세포질에서 Syph의 동일한 음전하를 유지한다는 점에서, 이번 연구 결과를 통해 단순한 전하 상호작용보다는 파이 양이온 정전기적 상호작용이 단백질들의 코아세르베이션에 관련이 있는 것으로 강력하게 시사하였다.

Syph와 Syn의 코아세르베이션을 지배하는 기전을 해명함으로써, 이번 연구는 분자적 과정에 대한 소중한 통찰력을 제공할 뿐만 아니라, 시냅스 활동 중 Syph와 Syn 사이의 다가 파이 양이온 정전기적 상호작용 조절이 시냅스 소포 군집화의 동적 특성에 기여할 수 있는 흥미로운 가능성을 제기하였다.

* 본 내용은 *Molecular Brain*에 출판 완료된 내용임.

주요어 : Synaptophysin, Synapsin, 액체-액체 상 분리, 파이 (*pi*)-양이온 상호작용, 시냅스 소낭 클러스터, 시냅스 전신경 말단

학번 : 2018-12556